Structural Engineering and Mechanics, *Vol. 64, No. 4 (2017) 449-459*
DOI: https://doi.org/10.12989/sem.2017.64.4.449

A Kalman filter based algorithm for wind load estimation on high-rise buildings

Lun-hai Zhi[1a], Pan Yu[1b], Jian-wei Tu[2c], Bo Chen[*2] and Yong-gui Li[3d]

[1]*School of Civil Engineering and Architecture, Wuhan University of Technology, Wuhan 430070, China*
[2]*Key Laboratory of Roadway Bridge and Structural Engineering, Wuhan University of Technology, Wuhan 430070, China*
[3]*School of Civil Engineering, Hunan University of Science and Technology, Xiangtan 411201, China*

(Received January 2, 2017, Revised June 26, 2017, Accepted July 10, 2017)

Abstract. High-rise buildings are generally sensitive to strong winds. The evaluation of wind loads for the structural design, structural health monitoring (SHM), and vibration control of high-rise buildings is of primary importance. Nevertheless, it is difficult or even infeasible to measure the wind loads on an existing building directly. In this regard, a new inverse method for evaluating wind loads on high-rise buildings is developed in this study based on a discrete-time Kalman filter. The unknown structural responses are identified in conjunction with the wind loads on the basis of limited structural response measurements. The algorithm is applicable for estimating wind loads using different types of wind-induced response. The performance of the method is comprehensively investigated based on wind tunnel testing results of two high-rise buildings with typical external shapes. The stability of the proposed algorithm is evaluated. Furthermore, the effects of crucial factors such as cross-section shapes of building, the wind-induced response type, errors of structural modal parameters, covariance matrix of noise, noise levels in the response measurements and number of vibration modes on the identification accuracy are examined through a detailed parametric study. The research outputs of the proposed study will provide valuable information to enhance our understanding of the effects of wind on high-rise buildings and improve codes of practice.

Keywords: force identification; wind load; high-rise building; Kalman filter; structural response; wind tunnel test

1. Introduction

Knowledge of wind excitation is of importance in structural design, structural health monitoring (SHM) and vibration control for high-rise buildings. In general, wind loads on a high-rise building are very difficult to be measured directly, since force transducers might not exist and/or the spatial distribution of wind load may be complicated. Consequently, indirect measurement techniques have to be used in order to establish the excitation from measured structural response.

The issue of forces identification can be regarded as an inverse problem. Stevens (1987), Sanchez *et al*. (2014) presented an overview of the force estimation for the discrete and continuous linear vibration system. Traditionally, the force identification problem has been solved in the frequency domain. The frequency domain methods of estimating forces often use the Fourier Transform (FT) to establish the relationship between the force and response via the Frequency Response Function (FRF). However, it is well known that the identification process requires the inverse FT to determine the time histories of the estimated forces. The inverse transform makes these methods difficult to identify impact transient forces. Conversely, the time domain methods allow us to obtain the time-varying forces at each specific time-step. Owing to the fact that it is easy to be applied in engineering practice, the time domain method is very popular in engineering application recently. Kammer (1998) proposed a time domain force identification approach for estimating the discrete input force acting on a structure based on the measured response and the system Markov parameters. Huang (2001) used the conjugate gradient method to estimate the unknown transient external forces in a damped system by utilizing displacement and velocity measurements. Nordström (2006) presented a time domain input estimation algorithm for linear time-variant systems. Mao *et al*. (2010) developed a force identification method for a linear system based on the precise time-step integration and Tikhonov regularization technique. Ding *et al*. (2013) proposed an inverse method based on average acceleration discrete algorithm. The approach is formulated in state space and Iterative Tikhonov regularization is employed for the force identification.

The Kalman filter, together with its basic variants, is one of the most widely applied tools in fields related to the statistical signal processing, system identification and damage detection. In recent years, the application of the Kalman filter has also been extended to the force identification. For example, Ma *et al*. (1998, 2003) adopted

∗Corresponding author, Professor
E-mail: whutbcchen@163.com
[a]Associate Professor
E-mail: zhilunhai1979@163.com
[b]M.S. Student
E-mail: ypwhut@163.com
[c]Professor
E-mail: waider1@163.com
[d]Associate Professor
E-mail: lyg313@126.com

ISSN: 1225-4568 (Print), 1598-6217 (Online)

the Kalman filter and a least-squares algorithm to estimate the input force of linear structural systems. This method requires a full state measurement, which might not be feasible in practice. Gillijns and De Moor (2007) presented a joint input-state estimation filter in which the input estimate is obtained from the innovation by least-squares estimation and the state estimation problem is transformed into a standard Kalman filtering problem. Hwang *et al*. (2009) developed a Kalman filtering based inverse method for estimating modal wind loads on a structure using limited measured responses of a structure. Kang *et al*. (2012) applied the approach to identify the modal wind load acting on a building with a tuned mass damper (TMD) during a typhoon. Niu *et al*. (2015), Zhi *et al*. (2015) also extended this continuous-time Kalman filter algorithm to determine the time histories of wind loads on high-rise structures. Lourens *et al*. (2012) suggested an augment Kalman filter (AKF) for the force identification in structural dynamics. A dual Kalman filter approach was employed by Azam *et al*. (2015) to estimate the unknown input and states of a linear state-space model based on a limited number of acceleration measurements. Naets *et al*. (2015) presented an analytical investigation on the stability of the Kalman filtering based force identification methods. The observations indicated that acceleration measurements may lead to an unstable filter.

Although several Kalman filter based approaches for force identification have been developed, literature review reveals that an indirect estimation for the wind loads acting on complex structures such as high-rise buildings has rarely been conducted in the past. Furthermore, in some previous works employing a Kalman filter based approach, the input estimates using velocity or acceleration measurements were highly affected by spurious low frequency components. This observation implies that these methods may be unstable. Thus, the stability performance of the Kalman filter based algorithms should be investigated. Recently, the authors proposed a novel force identification method using a discrete time Kalman filter. The approach can allow estimation of the unknown wind loads and structural responses of a high-rise building based on limited measurements of structural responses. In order to verify the accuracy of the inverse method, a preliminary study was already carried out by the authors (Zhi *et al*. 2016) based on the numerical simulations and the field measurements of the dynamic responses of Taipei 101 Tower. However, the wind-induced response data used in the preliminary study were not sufficient (numerical results of the dynamic responses of Taipei 101 Tower were collected at one wind direction only and the measured accelerations instead of wind loads were used to validate the reconstruction results). In this study, the analytical procedure is further improved and applied to the estimation of the wind loads on two high-rise buildings based on wind tunnel test results. Generally, the Kalman filter requires a priori knowledge of the measurement noise covariance matrix which significantly influences the accuracy of the force estimation. However, in the references mentioned above, the covariance matrix of the measurement noise is usually assumed to be diagonal matrices whose diagonal entries are specified as arbitrary values. Assuming arbitrary values for practical measurements may yield poor results. In this study, the *L*-curve method (Hansen 1992, Lourens *et al*. 2012, Amiri *et al*. 2015) will be employed to determine measurement noise covariance matrix for improving the accuracy of the force identification.

This paper proceeds as follows: Section 2 presents the Kalman filter based inverse method for the estimation of wind loads on high-rise buildings. In Section 3, the capacity of the proposed approach will be investigated based on the wind tunnel test results of two high-rise buildings. A particular attention is paid to the influences of several factors including the cross-section shape of a building, measurement noise, covariance matrix of noise, errors of structural modal parameters and the number of vibration modes, on the wind load estimation. Finally, some concluding remarks are summarized in Section 4.

2. Theory of wind load identification

2.1 Dynamic responses identification using Kalman filter

The governing equations of motion of a high-rise building with "*n*" floors subjected to wind loads can be written as

$$\boldsymbol{M}\ddot{\boldsymbol{y}} + \boldsymbol{C}\dot{\boldsymbol{y}} + \boldsymbol{K}\boldsymbol{y} = \boldsymbol{F} \tag{1}$$

where $\boldsymbol{M}$, $\boldsymbol{C}$ and $\boldsymbol{K}$ are the $n\times n$ mass, damping and stiffness matrices of the structure, respectively. $\boldsymbol{y}$, $\dot{\boldsymbol{y}}$ and $\ddot{\boldsymbol{y}}$ are the displacement, velocity and acceleration vectors of the structure, respectively. $\boldsymbol{F}$ is the wind force vector acting on the high-rise building.

By utilizing the mode superposition method, Eq. (1) can be rewritten as

$$\ddot{U}_i + 2\xi_i\omega_i\dot{U}_i + \omega_i^2 U_i = \boldsymbol{\Phi}_i^{\mathrm{T}}\boldsymbol{F} = f_i \tag{2}$$

where $\boldsymbol{\Phi}_i$ is the mass normalized modal shape of the *i*-th mode. U_i and f_i are the modal displacement and modal wind load of the *i*th mode, respectively. ω_i and ξ_i denote the modal frequency and damping ratio of the *i*th mode, respectively.

Eq. (2) can be converted to the state-space representation, and let

$$\boldsymbol{X}_i(t) = \begin{bmatrix} U_i & \dot{U}_i \end{bmatrix}^{\mathrm{T}} \tag{3}$$

The state and measurement equation of the structural system in continuous time can be written as

$$\dot{\boldsymbol{X}}_i(t) = \boldsymbol{A}_i\boldsymbol{X}_i(t) + \boldsymbol{B}_i f_i \tag{4-1}$$

$$\boldsymbol{Z}_i(t) = \boldsymbol{H}_i\boldsymbol{X}_i(t) + \boldsymbol{D}_i f_i \tag{4-2}$$

In which $\boldsymbol{A}_i = \begin{bmatrix} 0 & 1 \\ -\omega_i^2 & -2\xi_i\omega_i \end{bmatrix}$, $\boldsymbol{B}_i = \begin{bmatrix} 0 & 1 \end{bmatrix}^T$. $\boldsymbol{Z}_i(t)$ represents the measured modal response. The system matrices $\boldsymbol{H}_i$ and $\boldsymbol{D}_i$ are different, depending on the response utilized. In the case of displacement measurements, $\boldsymbol{H}_i$=[1

0] and $\boldsymbol{D}_i$=[0]. For acceleration measurements, the system matrices becomes $\boldsymbol{H}_i = \left[-\omega_i^2 \quad -2\xi_i\omega_i\right]$ and $\boldsymbol{D}_i$=[1].

For the filter implementation, the continuous time linear differential equations can be converted to discrete time differential equations using a small sample time Δt. The discrete state-space equations are given by

$$\boldsymbol{X}_i(k+1) = \boldsymbol{\Psi}_i \boldsymbol{X}_i(k) + \boldsymbol{\Gamma}_i f_i(k) \tag{5-1}$$

$$\boldsymbol{Z}_i(k) = \boldsymbol{H}_i \boldsymbol{X}_i(k) + \boldsymbol{D}_i f_i(k) \tag{5-2}$$

where $\boldsymbol{\Psi}_i$ denotes the 2×2 state transition matrix (=exp($\boldsymbol{A}_i\Delta t$)). $\boldsymbol{\Gamma}_i$ represents the 2×1 process noise matrix ($= \int_{k\Delta t}^{(k+1)\Delta t} \exp\{\boldsymbol{A}_i[(k+1)\Delta t - \tau]\}\boldsymbol{B}_i d\tau = \left[\boldsymbol{\Psi}_i - \boldsymbol{I}\right]\boldsymbol{A}_i^{-1}\cdot\boldsymbol{B}_i$).

In practice, the field measurements always include the responses from the measurement noise. Thus, Eq. (5-2) is rewritten as

$$\boldsymbol{Z}_i(k) = \boldsymbol{H}_i \boldsymbol{X}_i(k) + \boldsymbol{D}_i f_i(k) + \boldsymbol{\varepsilon}_i \tag{6}$$

where $\boldsymbol{\varepsilon}_i$ is the measurement noise vector of structural responses.

The vectors $f_i(k)$ and $\varepsilon_i(k)$ are assumed to be mutually uncorrelated, zero-mean, white random noise signals. Their covariances are also assumed known and represented by matrices $\boldsymbol{Q}_i$ and $\boldsymbol{R}_i$, respectively

$$E[f_i(k)] = 0\,,\; E[f_i(k) f_i^{\mathrm{T}}(j)] = \boldsymbol{Q}_i(k)\delta_{kj} \tag{7}$$

$$E[\boldsymbol{\varepsilon}_i(k)] = 0\,,\; E[\boldsymbol{\varepsilon}_i(k)\boldsymbol{\varepsilon}_i^{\mathrm{T}}(j)] = \boldsymbol{R}_i(k)\delta_{kj} \tag{8}$$

$$E[f_i(k)\boldsymbol{\varepsilon}_i^{\mathrm{T}}(j)] = 0 \tag{9}$$

$$\boldsymbol{Q}_i(k) = E(ff^T) = \boldsymbol{I} \tag{10-1}$$

$$\boldsymbol{R}_i(k) = E(\varepsilon_i\varepsilon_i^{\mathrm{T}}) = \gamma\boldsymbol{I} \tag{10-2}$$

in which $\boldsymbol{I}$ is an identity matrix. γ is an adjustment factor of noise.

Defining

$$\boldsymbol{V}_i(k) = \boldsymbol{D}_i f_i(k) + \boldsymbol{\varepsilon}_i(k) \tag{11}$$

Eq. (6) is rewritten as

$$\boldsymbol{Z}_i(k) = \boldsymbol{H}_i \boldsymbol{X}_i(k) + \boldsymbol{V}_i(k) \tag{12}$$

From Eqs.(7) and (9), yields

$$\begin{aligned} E[\boldsymbol{V}_i(k)] &= E[\boldsymbol{D}_i f_i(k) + \boldsymbol{\varepsilon}_i(k)] \\ &= \boldsymbol{D}_i E[f_i(k)] + E[\boldsymbol{\varepsilon}_i(k)] \\ &= \boldsymbol{0} \end{aligned} \tag{13}$$

$$\begin{aligned} E[\boldsymbol{V}_i(k)\boldsymbol{V}_i^{\mathrm{T}}(j)] &= E[\boldsymbol{D}_i f_i(k) f_i^{\mathrm{T}}(k)\boldsymbol{D}_i^{\mathrm{T}} + \boldsymbol{D}_i f_i(k)\boldsymbol{\varepsilon}_i^{\mathrm{T}}(k) \\ &\quad + \boldsymbol{\varepsilon}_i(k) f_i^{\mathrm{T}}(k)\boldsymbol{D}_i^{\mathrm{T}} + \boldsymbol{\varepsilon}_i(k)\boldsymbol{\varepsilon}_i^{\mathrm{T}}(j)] \\ &= [\boldsymbol{D}_i\boldsymbol{Q}_i(k)\boldsymbol{D}_i^{\mathrm{T}} + \boldsymbol{R}_i(k)]\delta_{kj} \\ &= \boldsymbol{r}_i(k)\delta_{kj} \end{aligned} \tag{14}$$

$$\begin{aligned} E[f_i(k)\boldsymbol{V}_i^{\mathrm{T}}(j)] &= E[f_i(k) f_i^{\mathrm{T}}(j)\boldsymbol{D}_i^{\mathrm{T}} + f_i(k)\boldsymbol{\varepsilon}_i^{\mathrm{T}}(j)] \\ &= \boldsymbol{Q}_i(k)\boldsymbol{D}_i^{\mathrm{T}}\delta_{kj} \\ &= \boldsymbol{S}_i(k)\delta_{kj} \end{aligned} \tag{15}$$

Hence, the stochastic processes $\boldsymbol{V}_i(k)$ is zero mean and white with covariance matrix $\boldsymbol{r}_i(k) = \boldsymbol{D}_i\boldsymbol{Q}_i(k)\boldsymbol{D}_i^{\mathrm{T}} + \boldsymbol{R}_i(k)$. Meanwhile, it is also conclude that the vector $f_i(k)$ is correlated with the stochastic processes $\boldsymbol{V}_i(k)$. This implies that the discrete-time system of Eqs. (5-1) and (12) cannot satisfy the classical Kalman filter equation and should be modified.

From Eq. (12), one obtains

$$\boldsymbol{Z}_i(k-1) - \boldsymbol{H}_i\boldsymbol{X}_i(k-1) - \boldsymbol{V}_i(k) = \boldsymbol{0} \tag{16}$$

Adding "zero term" $\boldsymbol{Z}_i(k-1) - \boldsymbol{H}_i\boldsymbol{X}_i(k-1) - \boldsymbol{V}_i(k)$ to the right-hand-side of Eq. (5-1), yields

$$\begin{aligned} \boldsymbol{X}_i(k) &= \boldsymbol{\Psi}_i\boldsymbol{X}_i(k-1) + \boldsymbol{\Gamma}_i f_i(k-1) \\ &\quad + \boldsymbol{J}_i(k-1)[\boldsymbol{Z}_i(k-1) - \boldsymbol{H}_i\boldsymbol{X}_i(k-1) - \boldsymbol{V}_i(k-1)] \\ &= [\boldsymbol{\Psi}_i - \boldsymbol{J}_i(k-1)\boldsymbol{H}_i]\boldsymbol{X}_i(k-1) + \boldsymbol{J}_i(k-1)\boldsymbol{Z}_i(k-1) \\ &\quad + \boldsymbol{\Gamma}_i f_i(k-1) - \boldsymbol{J}_i(k-1)\boldsymbol{V}_i(k-1) \end{aligned} \tag{17}$$

where $\boldsymbol{J}_i(k)$ is the a priori gain matrix.

Letting

$$\boldsymbol{\Psi}_i^* = \boldsymbol{\Psi}_i - \boldsymbol{J}_i(k-1)\boldsymbol{H}_i \tag{18}$$

$$\boldsymbol{W}_i(k-1) = \boldsymbol{\Gamma}_i f_i(k-1) - \boldsymbol{J}_i(k-1)\boldsymbol{V}_i(k-1) \tag{19}$$

It follows from Eq. (17) that

$$\boldsymbol{X}_i(k) = \boldsymbol{\Psi}_i^*\boldsymbol{X}_i(k-1) + \boldsymbol{J}_i(k-1)\boldsymbol{Z}_i(k-1) + \boldsymbol{W}_i(k-1) \tag{20}$$

in which

$$\begin{aligned} E[\boldsymbol{W}_i(k-1)] &= E[\boldsymbol{\Gamma}_i f_i(k) - \boldsymbol{J}_i(k)\boldsymbol{V}_i(k)] \\ &= \boldsymbol{\Gamma}_i E[f_i(k)] - \boldsymbol{J}_i(k)E[\boldsymbol{V}_i(k)] \\ &= \boldsymbol{0} \end{aligned} \tag{21}$$

Eq. (21) indicates that $\boldsymbol{W}_i(k)$ is a zero-mean stochastic process.

Based on Eqs. (11) and (19), one obtains

$$\begin{aligned} E[\boldsymbol{W}_i(k)\boldsymbol{V}_i^T(j)] &= E\left\{[\boldsymbol{\Gamma}_i f_i(k) - \boldsymbol{J}_i(k)\boldsymbol{V}_i(k)]\boldsymbol{V}_i^T(j)\right\} \\ &= \boldsymbol{\Gamma}_i E[f_i(k)\boldsymbol{V}_i^T(j)] - \boldsymbol{J}_i(k)E[\boldsymbol{V}_i(k)\;\boldsymbol{V}_i^T(j)] \\ &= [\boldsymbol{\Gamma}_i\boldsymbol{S}_i(k) - \boldsymbol{J}_i(k)\boldsymbol{r}_i(k)]\delta_{kj} \end{aligned} \tag{22}$$

By choosing

$$\boldsymbol{J}_i(k) = \boldsymbol{\Gamma}_i\boldsymbol{S}_i(k)[\boldsymbol{r}_i(k)]^{-1} \tag{23}$$

There has

$$E[\boldsymbol{W}_i(k)\boldsymbol{V}_i^T(j)] = \boldsymbol{0} \tag{24}$$

The expression in Eq. (24) indicates that the stochastic processes $\boldsymbol{W}_i(k)$ and $\boldsymbol{V}_i(k)$ are uncorrelated. It is clear that the choice of $\boldsymbol{J}_i(k)$ makes Eqs. (12) and (20) satisfy the classical Kalman filter equation.

Based on the Kalman filter for the discrete-time state space system of Eqs. (12) and (20), the estimated wind-induced responses $\hat{\boldsymbol{X}}_i(k)$ can be obtained by the following equations

$$\hat{\boldsymbol{X}}_i(k/k-1)=\boldsymbol{\Psi}_i\hat{\boldsymbol{X}}_i(k-1)+\boldsymbol{J}_i(k-1)[\boldsymbol{Z}_i(k-1)-\boldsymbol{H}_i\hat{\boldsymbol{X}}_i(k-1)] \tag{25}$$

$$\hat{\boldsymbol{X}}_i(k)=\hat{\boldsymbol{X}}_i(k/k-1)+\boldsymbol{G}_i(k)[\boldsymbol{Z}_i(k)-\boldsymbol{H}_i\hat{\boldsymbol{X}}_i(k/k-1)] \tag{26}$$

$$\boldsymbol{J}_i(k-1)=\boldsymbol{\Gamma}_i\boldsymbol{Q}_i(k-1)\boldsymbol{D}_i^{\mathrm{T}}[\boldsymbol{D}_i\boldsymbol{Q}_i(k-1)\boldsymbol{D}_i^{\mathrm{T}}+\boldsymbol{R}_i(k-1)]^{-1} \tag{27}$$

$$\begin{aligned}\boldsymbol{P}_i(k/k-1)=&[\boldsymbol{\Psi}_i-\boldsymbol{J}_i(k-1)\boldsymbol{H}_i]\boldsymbol{P}_i(k-1)[\boldsymbol{\Psi}_i-\boldsymbol{J}_i(k-1)\boldsymbol{H}_i]^{\mathrm{T}}\\&+\boldsymbol{\Gamma}_i\boldsymbol{Q}_i(k-1)\boldsymbol{\Gamma}_i^{\mathrm{T}}-\boldsymbol{J}_i(k-1)\boldsymbol{D}_i\boldsymbol{Q}_i(k-1)\boldsymbol{\Gamma}_i^{\mathrm{T}}\end{aligned} \tag{28}$$

$$\begin{aligned}\boldsymbol{G}_i(k)=&\boldsymbol{P}_i(k/k-1)\boldsymbol{H}_i^{\mathrm{T}}[\boldsymbol{H}_i\boldsymbol{P}_i(k/k-1)\boldsymbol{H}_i^{\mathrm{T}}\\&+\boldsymbol{D}_i\boldsymbol{Q}_i(k)\boldsymbol{D}_i^{\mathrm{T}}+\boldsymbol{R}_i(k)]^{-1}\end{aligned} \tag{29}$$

$$\boldsymbol{P}_i(k)=[\boldsymbol{I}-\boldsymbol{G}_i(k)\boldsymbol{H}_i]\boldsymbol{P}_i(k/k-1) \tag{30}$$

where $\boldsymbol{G}_i(k)$ denotes the Kalman filter gain matrix at time instant k; $\boldsymbol{P}_i(k)$ denotes the error covariance matrix of the filter. The filter is initialized as follows

$$\hat{\boldsymbol{X}}_i(0)=E[\boldsymbol{X}_i(0)] \tag{31}$$

$$\boldsymbol{P}_i(0)=E\{[\boldsymbol{X}_i(0)-\hat{\boldsymbol{X}}_i(0)][\boldsymbol{X}_i(0)-\hat{\boldsymbol{X}}_i(0)]^{\mathrm{T}}\} \tag{32}$$

2.2 Structural response and wind load estimation

Substituting the estimated wind-induced response $\hat{\boldsymbol{X}}_i(k)$ into Eq. (5-1), yields

$$\boldsymbol{\Gamma}_i\hat{f}_i(k)=\hat{\boldsymbol{X}}_i(k+1)-\boldsymbol{\Psi}_i\hat{\boldsymbol{X}}_i(k) \tag{33}$$

where $\hat{f}_i(k)$ denotes the estimated modal wind loads of the ith mode.

Premultiplying each term in Eq. (33) by $\boldsymbol{\Gamma}_i^T$ gives

$$\boldsymbol{\Gamma}_i^T\boldsymbol{\Gamma}_i\hat{f}_i(k)=\boldsymbol{\Gamma}_i^T\left[\hat{\boldsymbol{X}}_i(k+1)-\boldsymbol{\Psi}_i\hat{\boldsymbol{X}}_i(k)\right] \tag{34}$$

From Eq. (5-2) it is concluded that $\left(\boldsymbol{\Gamma}_i^T\cdot\boldsymbol{\Gamma}_i\right)$ is a real number. Eq. (34) can be rewritten as

$$\hat{f}_i(k)=\left(\boldsymbol{\Gamma}_i^T\boldsymbol{\Gamma}_i\right)^{-1}\cdot\boldsymbol{\Gamma}_i^T\cdot[\hat{\boldsymbol{X}}_i(k+1)-\boldsymbol{\Psi}_i\hat{\boldsymbol{X}}_i(k)] \tag{35}$$

Finally, the first q modal wind loads $\hat{f}_i(k)(i=1,2,\cdots,q)$ can be estimated from the corresponding decomposed modal responses, respectively.

Based on Eq. (2), it has

$$\mathbf{F}=\left[(\boldsymbol{\Phi}_{n\times n})^{\mathrm{T}}\right]^{-1}\left[f_1\quad f_2\quad\cdots\quad f_n\right]^{\mathrm{T}} \tag{36}$$

Defining

$$\varphi_{n\times n}=\left[\varphi_1\quad\varphi_2\quad\cdots\quad\varphi_n\right]=[(\boldsymbol{\Phi}_{n\times n})^{\mathrm{T}}]^{-1} \tag{37}$$

Eq. (36) is rewritten as

$$\begin{aligned}\boldsymbol{F}=&\left[\varphi_1\quad\varphi_2\quad\cdots\quad\varphi_n\right]\left[f_1\quad f_2\quad\cdots\quad f_n\right]^{\mathrm{T}}\\=&\sum_{i=1}^{n}\varphi_i\ f_i\end{aligned} \tag{38}$$

Considering the mass normalization condition: $M_i=\boldsymbol{\Phi}_i^{\mathrm{T}}\boldsymbol{M}\boldsymbol{\Phi}_i=1\ \ (i=1,2,\cdots,n)$, Eq. (37) can be rewritten as

$$\varphi_{n\times n}=[(\boldsymbol{\Phi}_{n\times n})^{\mathrm{T}}]^{-1}=\mathbf{M}\,\boldsymbol{\Phi}_{n\times n} \tag{39}$$

Owing to the fact that the dynamic behavior of the high-rise building is governed by the first few mode responses, the fluctuating wind load and wind-induced responses are approximately given by

$$\hat{\boldsymbol{F}}=\sum_{i=1}^{q}\varphi_i\ \hat{f}_i=\varphi_{n\times q}\ \hat{\boldsymbol{f}}_{q\times 1} \tag{40}$$

$$\begin{cases}\hat{\boldsymbol{y}}_{n\times 1}=\boldsymbol{\Phi}_{n\times q}\ \hat{\boldsymbol{U}}_{q\times 1}\\ \hat{\dot{\boldsymbol{y}}}_{n\times 1}=\boldsymbol{\Phi}_{n\times q}\ \hat{\dot{\boldsymbol{U}}}_{q\times 1}\\ \hat{\ddot{\boldsymbol{y}}}_{n\times 1}=\boldsymbol{\Phi}_{n\times q}\ \hat{\ddot{\boldsymbol{U}}}_{q\times 1}\end{cases} \tag{41}$$

where $\varphi_{n\times q}=\mathbf{M}\,\boldsymbol{\Phi}_{n\times q}$.

Furthermore, it is note that the proposed inverse method requires a prior assumption on the knowledge of the structural parameters (damping ratios, mode shapes and natural frequencies) of the first few vibration modes and the structural mass matrix.

2.3 Stability properties of the inverse method

The proposed approach can estimate the wind loads and unknown structural responses using limited structural response measurements. In practice, acceleration responses are most convenient to be measured among the structural dynamic responses. However, previous studies show the inadequacy of many Kalman filter based approaches using only acceleration measurements to provide stable results (Lourens *et al*. 2012, Naets *et al*. 2015, Azam *et al*. 2015). According to Simon's (2006) observations, a steady-state Kalman filter can be expressed as

$$\hat{\boldsymbol{X}}_i(k)=\hat{\boldsymbol{X}}_i(k/k-1)+\boldsymbol{G}_i(\infty)[\boldsymbol{Z}_i(k)-\boldsymbol{H}_i\hat{\boldsymbol{X}}_i(k/k-1)] \tag{42}$$

Substituting Eq. (25) into the above equation, Eq. (42) can be written as

$$\begin{aligned}\hat{\boldsymbol{X}}_i(k)=&[\boldsymbol{I}-\boldsymbol{G}_i(\infty)\boldsymbol{H}_i][\boldsymbol{\Psi}_i-\boldsymbol{J}_i\boldsymbol{H}_i]\hat{\boldsymbol{X}}_i(k-1)\\&+[\boldsymbol{I}-\boldsymbol{G}_i(\infty)\boldsymbol{H}_i]\boldsymbol{J}_i\boldsymbol{Z}_i(k-1)+\boldsymbol{G}_i(\infty)\boldsymbol{Z}_i(k)\end{aligned} \tag{43}$$

where

$$\boldsymbol{G}_i(\infty)=\boldsymbol{P}_i(\infty)\boldsymbol{H}_i^{\mathrm{T}}[\boldsymbol{H}_i\boldsymbol{P}_i(\infty)\boldsymbol{H}_i^{\mathrm{T}}+\boldsymbol{D}_i\boldsymbol{Q}_i(k)\boldsymbol{D}_i^{\mathrm{T}}+\boldsymbol{R}_i(k)]^{-1} \tag{44}$$

Steady-state Kalman gain $\boldsymbol{G}_i(\infty)$ can be obtained from the following discrete Riccati equation

$$\begin{aligned}\boldsymbol{P}_i(\infty)=&[\boldsymbol{\Psi}_i-\boldsymbol{J}_i\boldsymbol{H}_i]\{\boldsymbol{I}-\boldsymbol{P}_i(\infty)\boldsymbol{H}_i^{\mathrm{T}}[\boldsymbol{H}_i\boldsymbol{P}_i(\infty)\boldsymbol{H}_i^{\mathrm{T}}+\boldsymbol{D}_i\boldsymbol{Q}_i(k)\boldsymbol{D}_i^{\mathrm{T}}\\&+\boldsymbol{R}_i(k)]^{-1}\boldsymbol{H}_i\}\boldsymbol{P}_i(\infty)[\boldsymbol{\Psi}_i-\boldsymbol{J}_i\boldsymbol{H}_i]^T+\boldsymbol{\Gamma}_i\boldsymbol{Q}_i(k)\boldsymbol{\Gamma}_i^{\mathrm{T}}-\boldsymbol{J}_i\boldsymbol{D}_i\boldsymbol{Q}_i(k)\boldsymbol{\Gamma}_i^{\mathrm{T}}\end{aligned} \tag{45}$$

If the matrix $[\boldsymbol{I}-\boldsymbol{G}_i(\infty)\boldsymbol{H}_i][\boldsymbol{\Psi}_i-\boldsymbol{J}_i\boldsymbol{H}_i]$ satisfies the criterion

$$\rho=\left|\eta_j\right|_{\max}<1 \tag{46}$$

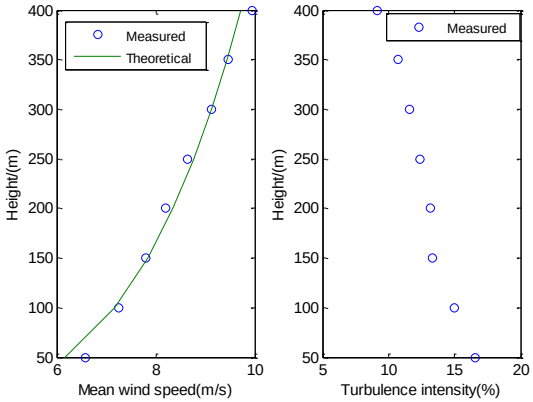

Fig. 1 Mean wind speed and turbulence intensity profiles

(a) Building A

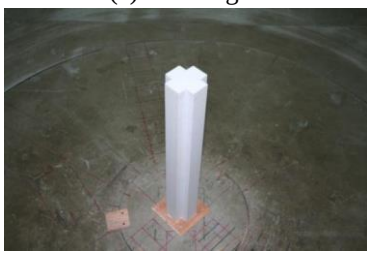

(b) Building B

Fig. 2 Models for wind tunnel test

the Kalman filter for a structural system is stable, where η_j denotes the eigenvalue of the matrix $[\boldsymbol{I}-\boldsymbol{G}_i(\infty)\boldsymbol{H}_i][\boldsymbol{\Psi}_i-\boldsymbol{J}_i\boldsymbol{H}_i]$. In this study, the stability performance of the above proposed algorithm will be performed to evaluate by Eq. (46) based on two types of response measurements, namely, displacement and acceleration responses.

3. Verification of wind load identification using wind tunnel test data

3.1 Experiment set and test model

To evaluate the feasibility of the new inverse method, the algorithm will be applied to the identification of wind loads on high-rise buildings with typical shapes based on wind tunnel test results. In the validation study, the wind loading at each measurement elevation on a high-rise building model is known through simultaneous pressure measurements in wind tunnel tests. This will allow a proper comparison of the wind-induced responses and the wind loads determined by the proposed inverse method with those of the wind tunnel tests.

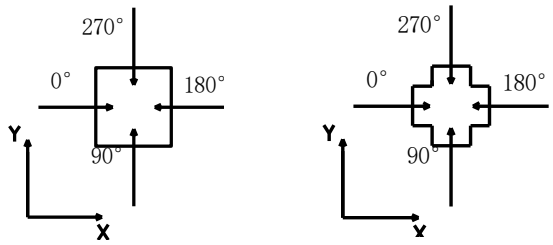

(a) Building A (b) Building B

Fig. 3 Coordinate system

Wind tunnel tests were conducted in the boundary layer wind tunnel laboratory at Hunan University, China. The wind tunnel has a test section 17 m long with a cross-section of 2.5 m×3 m. In accordance with the Chinese National Load Code (GB50009-2012), the exposure category C (corresponding to the exponent of the power law of mean speed profile of 0.22) is simulated at a length scale of 1/500 in the test area. The simulated profiles of mean wind speed and turbulence intensity are shown in Fig. 1. Two building models with different cross-section shapes (square and corner-modified square cross-section shape), designated Building A and Building B, are chosen as examples. Each building model is 10 cm by 10 cm, and 60 cm high, as shown in Fig. 2. Both models have the same length scale with that of wind simulation, i.e., 1/500, representing a real building of a height of 300 m.

In the wind tunnel test, wind direction was changed at intervals of 15° for each case, as displayed in Fig. 3. The pressure data were collected using an electronic pressure scanner system made by Scanivalve Inc. (USA). The data sampling frequency was 312.5 Hz and the sampling length was 30s. Two high-rise buildings are assumed to be 68 stories above ground and located in the central district of Guangzhou, China. The wind speed at a height of 10 m with a 100-year return period in Guangzhou is 30.5 m/s as specified in the Chinese National Load Code (GB50009-2012). The time-histories of wind forces at each measurement elevation with a 100-year return period were computed by integrating the wind pressures on the buildings.

3.2 Structural responses and wind load identification

Generally, it is impossible to directly measure the wind-induced responses of a high-rise building through simultaneous pressure measurements in wind tunnel tests. Hence, time history analysis is performed to determine the wind-induced responses of high-rise buildings based on the measured fluctuating wind loads from wind tunnel tests. The analytical responses will be used as the "measured" wind-induced responses in the inverse analysis. The system matrices (mass and stiffness) of two high-rise buildings are established based on the finite element model, respectively. The Rayleigh damping expressed in the following form is adopted as

$$\boldsymbol{C}=\alpha\cdot\boldsymbol{M}+\beta\cdot\boldsymbol{K} \tag{47}$$

Table 1 The first six natural frequencies of the Building A (Hz)

Direction	Mode 1	Mode 2	Mode 3	Mode 4	Mode 5	Mode 6
X	0.189	0.436	0.692	0.945	1.211	1.454
Y	0.198	0.457	0.726	0.991	1.270	1.545

Table 2 The first six natural frequencies of the Building B (Hz)

Direction	Mode 1	Mode 2	Mode 3	Mode 4	Mode 5	Mode 6
X	0.163	0.377	0.599	0.818	1.049	1.259
Y	0.171	0.396	0.629	0.858	1.100	1.320

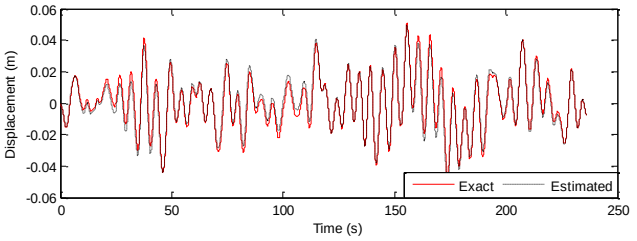

(a) Displacement

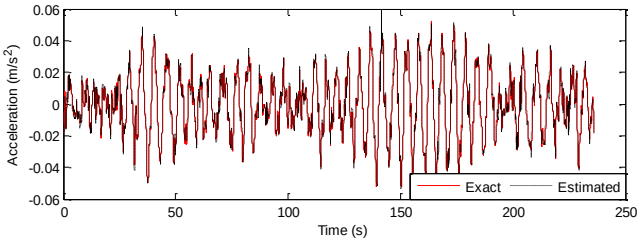

(b) Acceleration

Fig. 4 Comparison of time-histories of displacement and acceleration responses at the 60th floor in direction *X* under wind direction of 0°, Building A

where α and β are constants to be determined from the damping ratios ξ_1, ξ_2 and natural frequencies ω_1, ω_2 of the first two vibration modes. The damping ratio of both buildings is assumed to be 5%.

In order to obtain an accurate reduced-order representation of wind-induced responses, the required energy contribution of the selected governing modes should exceed 99% of the total energy of the structural response (Hwang *et al*. 2009, Zhi *et al*. 2015, 2016). The proper orthogonal decomposition (POD) technique is adopted to obtain the governing modes of the example high-rise structures in this study. It is observed from the analytical results that the summation of the first six modes' energy contribution of two high-rise buildings exceeds 99%. Thus, the number of modes of both structures considered in this study is six, as listed in Tables 1 and 2. Furthermore, the stability performance of the proposed algorithm is also evaluated by Eq. (46). The calculated values of ρ for the displacement and acceleration measurements are all smaller than 1. It is thus concluded that the stability of the proposed algorithm can be guaranteed for two types of response measurements.

In this section, time-histories of structural responses at the 18th, 24th, 36th, 53rd, 59th and 68th floors where the

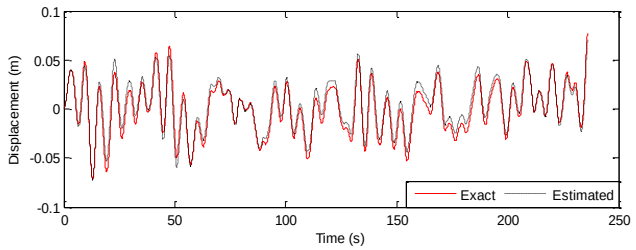

(a) Displacement

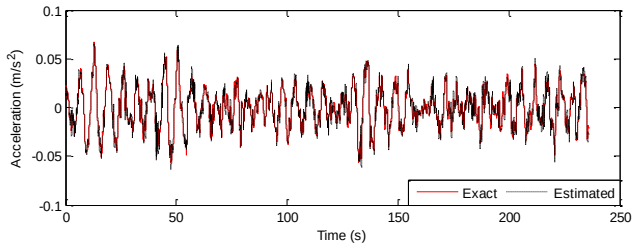

(b) Acceleration

Fig. 5 Comparison of time-histories of displacement and acceleration responses at the 60th floor in direction *X* under wind direction of 0°, Building B

vibration amplitudes or where the changes of the vibration mode shape are relatively large, are used to estimate the wind excitation with the force identification method (Li *et al*. 2004). It is noted that only the fluctuating wind loads on high-rise buildings are identified based on the limited wind-induced responses. On the basis of the acceleration responses at the six floors, the dynamic responses at the other floors are identified by the load estimation technique (Assuming $\gamma=10^{-8}$). Figs. 4 and 5 display the time-histories of the identified displacement and velocity responses at the 60th floor in *X* direction for buildings *A* and *B* under an approaching wind direction of 0°, respectively. For the purposes of comparison, the corresponding exact wind-induced responses of both buildings, which are calculated by the response analysis based on the wind tunnel test results, are also presented in these figures. It is seen that the identified displacement and velocity responses of two buildings are very close to the corresponding exact wind-induced responses. This indicates that the proposed inverse method can satisfactorily predict the unmeasured wind-induced responses of two different cross-section high-rise buildings.

Figs. 6 and 7 refer to the comparisons between the identified and exact total wind forces (base shear forces) on buildings *A* and *B* in directions *X* and *Y*, respectively, based on the displacement and acceleration responses. It is seen from these figures that the time-histories of the identified total wind forces in *Y* direction (across-wind direction) for both building agree well with their corresponding exact results, whereas there are slight differences between the estimated and exact total wind forces in *X* direction (along-wind direction). This observation may be attributable to several reasons including the different mechanisms of generating the two types of forces. Tables 3 and 4 present the Root Mean Square (RMS) values of the estimated total wind forces in both directions for two example buildings with approaching wind directions of 0°, 45° and 90°,

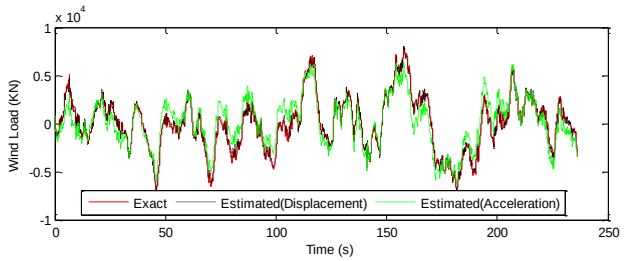

(a) Direction *X*

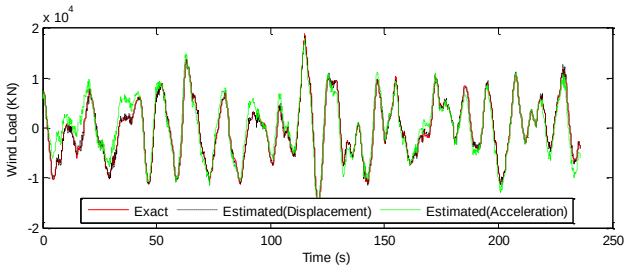

(b) Direction *Y*

Fig. 6 Time histories of the total wind loads on Building A under wind direction of 0°

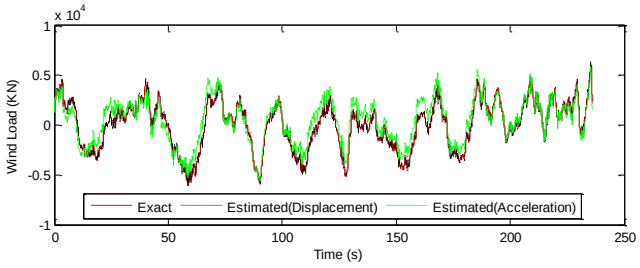

(a) Direction *X*

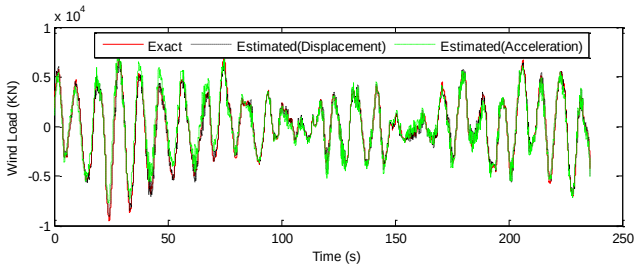

(b) Direction *Y*

Fig. 7 Time histories of the total wind loads on Building B under wind direction of 0°

respectively. The data in the tables indicate that all the differences between the identified and exact RMS wind forces for two different cross-section high-rise buildings are very small, and the largest error value is about 9.3%. The errors in the identified results from the acceleration measurements are a little larger than those from displacement measurements. The comparison observations indicate that the inverse approach proposed in this study can be applicable in engineering practice.

3.3 Effect of structural modal parameter error

An accurate determination of structural modal parameters is very important in exactly estimating wind loads and wind-induced responses of high-rise structures. However, many previous studies (Zhi *et al*. 2011, Li *et al*. 2011, 2014) demonstrated that structural modal parameters predicted by the finite element method (FEM) may exhibit departure from those measured in field measurements. Therefore, there is a need to assess the effects of modal parameter errors on the identification quality of the wind loads on high-rise buildings.

In this study, only the error of damping ratio which is set to be ±5% is taken into consideration. Fig. 8 shows the power spectral density (PSD) of the estimated total wind loads on building A with ±5% errors in damping ratio based on the acceleration responses. It is observed that the identified results for wind forces are very accurate. Though there are small differences between the estimated and exact wind force spectra in the low-frequency range, the identification quality is still satisfactory. Meanwhile, similar characteristics of the identified wind force are observed for the building B as shown in Fig. 9. This implies that the identified wind forces on two different cross-section high-

Table 3 RMS values of the estimated and exact wind loads on Building A

	Direction	Wind direction	Estimated (kN)	Exact (kN)	*Difference
Displacement feedback	*X*	0°	3457	3519	1.8%
		45°	2770	2816	1.6%
		90°	9120	9212	1.0%
	Y	0°	7524	7600	1.0%
		45°	3200	3244	1.4%
		90°	3404	3473	2.0%
Acceleration feedback	*X*	0°	3206	3519	8.9%
		45°	2563	2816	9.0%
		90°	9245	9212	-0.4%
	Y	0°	7519	7600	1.1%
		45°	2962	3244	8.7%
		90°	3160	3473	9.0%

* Difference=(Exact- Estimated)/Exact.

Table 4 RMS values of the estimated and exact wind loads on Building B

	Direction	Wind direction	Estimated (kN)	Exact (kN)	*Difference
Displacement feedback	*X*	0°	2999	3038	1.3%
		45°	3473	3587	3.2%
		90°	3369	3419	1.5%
	Y	0°	3797	3920	3.1%
		45°	3787	3883	2.5%
		90°	3124	3125	0
Acceleration feedback	*X*	0°	2864	3038	5.7%
		45°	3274	3587	8.7%
		90°	3315	3419	3.0%
	Y	0°	3710	3920	5.4%
		45°	3553	3883	8.5%
		90°	2834	3125	9.3%

* Difference = (Exact- Estimated)/Exact.

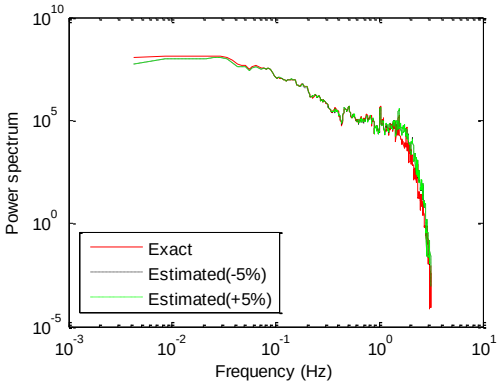

(a) Direction X

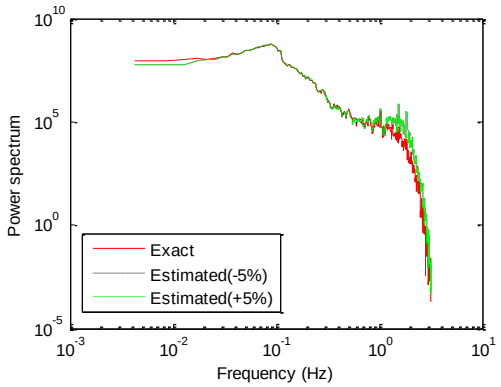

(b) Direction Y

Fig. 8 The PSD of the total wind loads on Building A for ±5% errors in damping ratio under wind direction of 0°

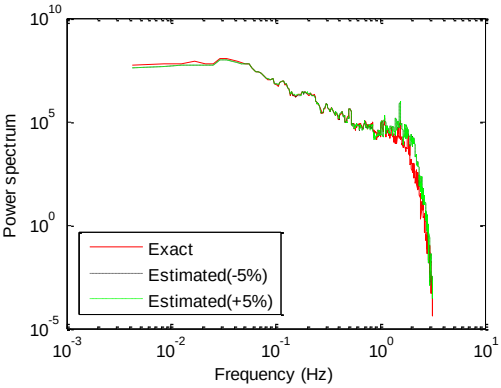

(a) Direction X

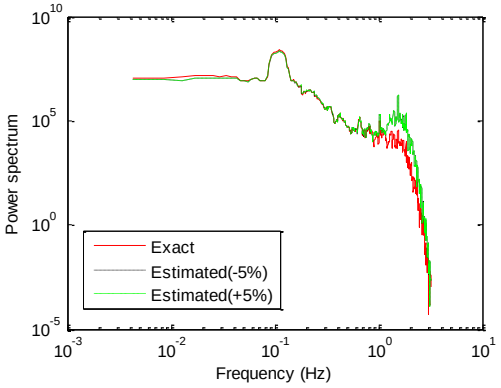

(b) Direction Y

Fig. 9 The PSD of the total wind loads on Building B for ±5% errors in damping ratio under wind direction of 0°

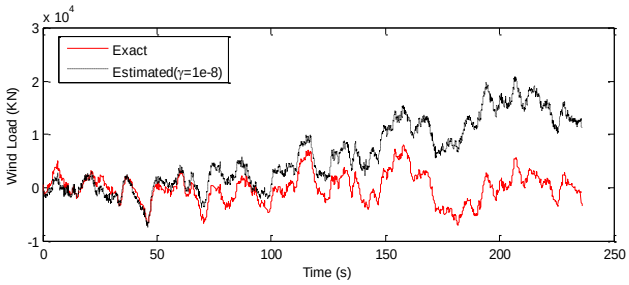

Fig. 10 Time histories of the total wind loads on Building A in direction X under wind direction of 0° (Noise level=5%)

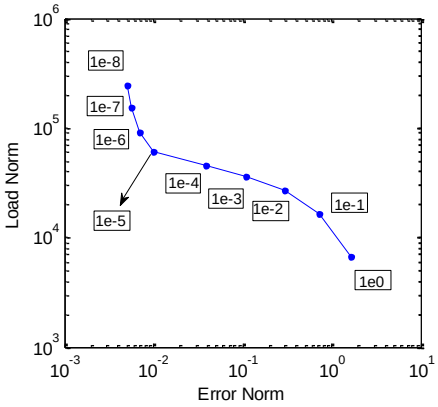

Direction X

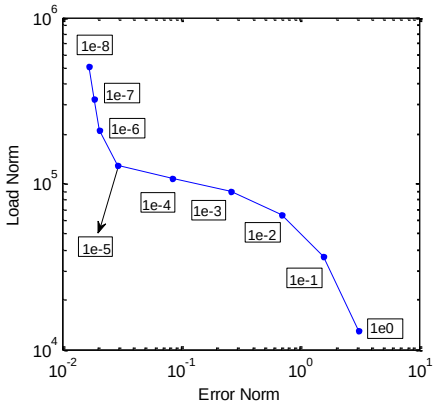

Direction Y

Fig. 11 The L-curve (Building A, Noise level=5%)

rise buildings by the inverse method are not sensitive to the errors of damping ratio.

3.4 Effect of noise on the identification

Noise contamination in measured signals is inevitable in practical engineering measurement. To investigate effects of the measurement noise on the performance of the inverse method, the white noise is added to the exact wind-induced responses, as follows

$$\boldsymbol{d}_{measured} = \boldsymbol{d}_{exact} + E_p \boldsymbol{Noise}\sigma(\boldsymbol{d}_{exact}) \tag{48}$$

where $\boldsymbol{d}_{measured}$ is the "measured" response. $\boldsymbol{d}_{exact}$ is the exact response. E_p is the percentage noise level. ***Noise*** denotes a standard normal distribution with zero mean and unit

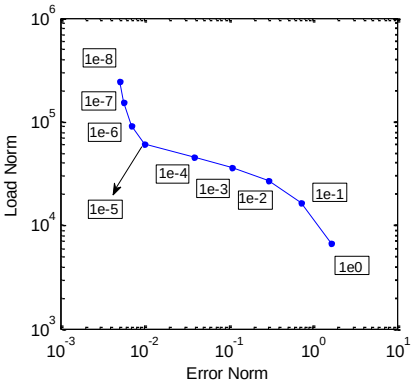

Direction *X*

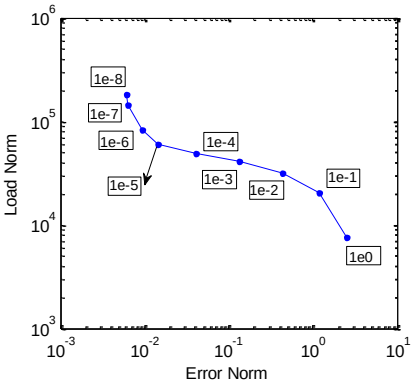

Direction *Y*

Fig. 12 The *L*-curve (Building B, Noise level=5%)

standard deviation. $\sigma(\boldsymbol{d}_{exact})$ is the standard deviation of the exact response.

In this section, 5% noise level is considered. When the same value of γ (=10^{-8}) as above is employed, the identified results by the acceleration feedback are shown in Fig. 10. It is found that there are obvious differences between the estimated and exact wind loads.

This could be attributed to that the value of γ employed in the previous sections is unreasonable for the wind force identification using the acceleration responses with measurement noise. In order to improve the accuracy of the wind load estimation, the *L*-curve criterion is employed to determine the optimal value of γ in this study. The *L*-curve plot displays an *L*-shaped appearance with a distinct corner separating the vertical part wind load norm ($\sum_{k=1}^{N}\left\|\hat{\boldsymbol{F}}\right\|_2$) and the horizontal part Error norm ($\sum_{k=1}^{N}\left\|\boldsymbol{y}_{measured}-\hat{\boldsymbol{y}}\right\|_2$, where $\hat{\boldsymbol{y}}$ are the estimated dynamic responses at the measurement locations) on a log-log scale. The corner of *L*-curve corresponds to the optimum parameter γ. Figs. 11 and 12 present the curves for the wind load identification using the acceleration responses with 5% noise level. It is clear that the curves have the typical aspect of an *L*-curve. The optimum parameters γ, which occur at the corner are then obtained. Using these optimum parameters γ, the PSD of the identified wind loads on the two example buildings from the acceleration responses with a 5% noise level are demonstrated in Figs. 13 and 14, respectively. The

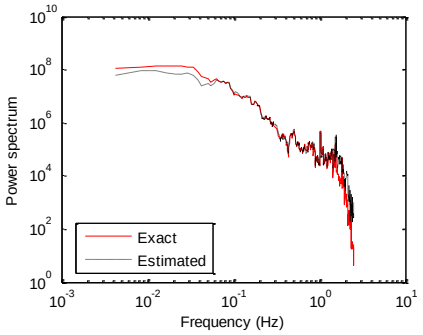

(a) Direction *X*

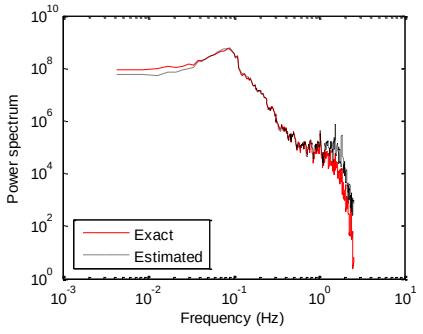

(b) Direction *Y*

Fig. 13 The PSD of the total wind loads on Building A under wind direction of 0° (Noise level=5%)

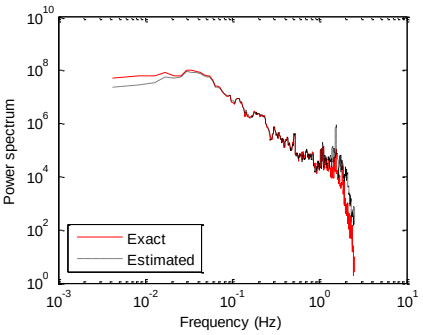

(a) Direction *X*

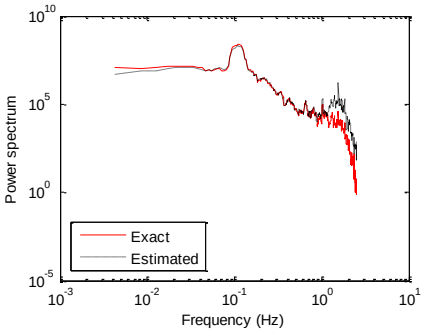

(b) Direction *Y*

Fig. 14 The PSD of the total wind loads on Building B under wind direction of 0° (Noise level=5%)

identified wind force spectra obtained by the inverse method with the *L*-curve criterion all agree well with the exact wind force spectra. This observation indicates that the proposed identification approach is robust against measurement noise.

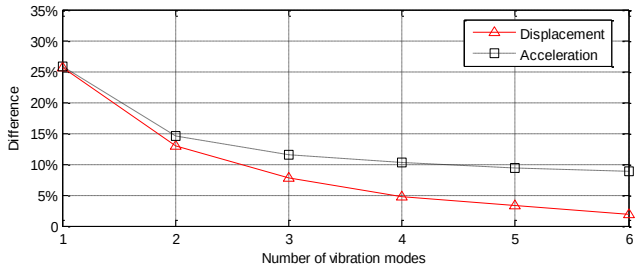

(a) Direction *X*

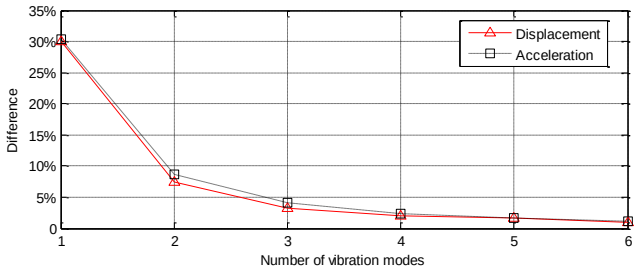

(b) Direction *Y*

Fig. 15 Differences between the exact RMS wind forces and the identified RMS wind loads from different number of vibration modes (Building A)

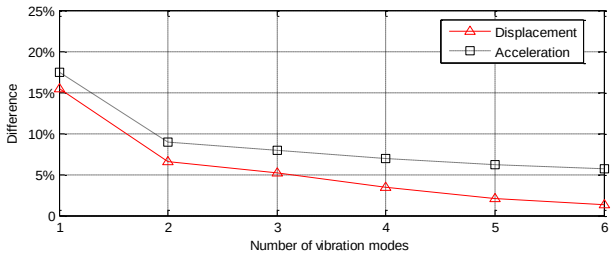

(a) Direction *X*

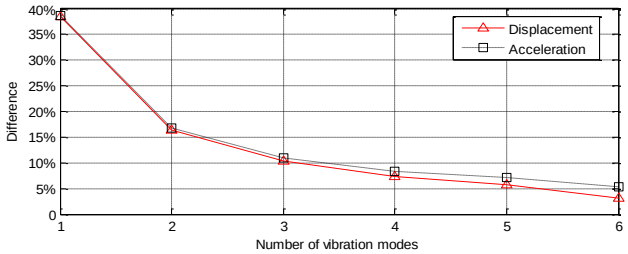

(b) Direction *Y*

Fig. 16 Differences between the exact RMS wind forces and the identified RMS wind loads from different number of vibration modes (Building B)

3.5 Effect of the number of vibration modes

The effect of the selected number of vibration modes on the identification accuracy is also investigated. The displacement and acceleration responses obtained from wind tunnel tests by considering different numbers of modes are used to identify wind loads acting on high-rise buildings. Figs. 15 and 16 displays the difference between the exact RMS wind forces and the identified RMS wind forces with different number of modes under 0^o wind direction. It is observed from the figures that the errors of the identified results for the two example buildings decrease with the increasing mode number. Higher mode contributions have significant effects on the wind force identification quality. The identified results also illustrate that the selected number of vibration modes determined by the POD technique is reasonable and the wind loads estimation for two buildings can be accurately carried out by the first six vibration modes.

4. Conclusions

A state-space model for structural systems and a Kalman filter-based inverse method are established in this study to identify the wind loads and wind-induced responses of high-rise buildings using limited measurements of structural responses. The *L*-curve criterion is further developed to determine the measurement noise covariance matrix which significantly influences the accuracy of the wind force identification. Wind tunnel experiments on the models of two different cross-section high-rise buildings are conducted to examine the effectiveness of the proposed method.

The experimental observations demonstrate that both types of response measurements (displacement or acceleration) can provide stable results. The estimated wind-induced responses are in accordance with the exact responses. Good agreements between the time histories of the identified and exact wind forces on two different cross-section buildings can be achieved. The displacement feedback is more accurate in estimating the wind loads than the acceleration feedback. The verification and validation observations also indicate that the wind loads acting on the high-rise buildings can be identified fairly accurately with structural modal parameters error. The *L*-curve criterion is capable of improving the efficiency of the proposed approach and satisfactory identified quality can be obtained even when considering noise contamination in dynamic responses. The number of vibration modes has obvious effect on the accuracy of the wind force identification and can be determined by using the POD technique. Therefore, it is concluded that the proposed inverse approach is an effective tool for estimating the wind loads on high-rise buildings based on limited structural responses.

As mentioned in previous sections, a Kalman filter based approach may be affected by spurious low frequency components using the acceleration measurement. Although the stability performance of the proposed algorithm has been evaluated in this study, further investigations on this topic should be conducted by using other methods (for example, the dual Kalman filter method proposed by Azam *et al*. 2015) in future works.

Acknowledgements

The work described in this paper was fully supported by grants from the National Natural Science Foundation of China (51478371, 51578434), the Fundamental Research Funds for the Central Universities (2017II30GX, 175206006), the Fok Ying Tong Education Foundation

(141074) and the Natural Science Foundation of Hubei Province (2016CFA020). The financial support is gratefully acknowledged.

Reference

Amiri, A.K. and Bucher, C. (2015), "Derivation of a new parametric impulse response matrix utilized for nodal wind load identification by response measurement", *J. Sound Vib.*, **344**, 101-113.

Azam, S.E., Chatzi, E. and Papadimitriou, C. (2015), "A dual Kalman filter approach for state estimation via output-only acceleration measurements", *Mech. Syst. Signal Pr.*, **60-61**,866-886.

Azam, S.E., Chatzi, E., Papadimitriou, C. and Smyth, A.W. (2015), "Experimental validation of Kalman-type filters for online and real-time state and input estimation", *J. Vib. Control*, **23**(15), 2494-2519.

Ding, Y., Law, S.S., Wu, B., Xu, G.S., Lin, Q., Jiang, H.B. and Miao, Q.S. (2013), "Average acceleration discrete algorithm for force identification in state space", *Eng. Struct.*, **56**, 1880-1892.

GB50009-2012 (2012), *Load Code for the Design of Building Structures*, China Architecture & Building Press, Beijing.

Gillijns, S. and De Moor, B. (2007), "Unbiased minimum-variance input and state estimation for linear discrete-time systems with direct feedthrough", *Automatica*, **43**, 934-937.

Hansen, P.C. (1992), "Analysis of discrete ill-posed problems by means of the L-curve", *Soc. Indust. Appl. Math.*, **34**,561-580.

Huang, C.H. (2001), "An inverse non-linear force vibration problem of estimating the external forces in a damped system with time-dependent system parameters", *J. Sound Vib.*, **242**(5), 749-765.

Hwang, J.S., Kareem, A. and Kim, H. (2009), "Estimation of modal loads using structural response", *J. Sound Vib.*, **326**, 522-539.

Kammer, D.C. (1998), "Input force reconstruction using a time domain technique", *J. Vib. Acoust.*, **120**(4), 868-874.

Kang, N., Kim, H., Choi, S., Jo, S., Hwang, J.S. and Yu, E. (2012), "Performance evaluation of TMD under typhoon using system identification and inverse wind load estimation", *Comput.Aid. Civil Infrastr. Eng.*, **27**, 455-473.

Lei, Y., Zhou, H. and Lai, Z.L. (2016), "A computationally efficient algorithm for real-time tracking the abrupt stiffness degradations of structural elements", *Comput.Aid. Civil Infrastr. Eng.*, **31**(6), 465-480.

Li, Q.S., Zhi, L. H., Yi, J., To, A. and Xie, J.M. (2014), "Monitoring of typhoon effects on a super-tall building in Hong Kong", *Struct. Control Hlth. Moni.*, **21**(6), 926-949.

Li, Q.S., Zhi, L.H., Tuan, A.Y., Kao, S.H., Su, S.C. and Wu, C.F. (2011), "Dynamic behavior of Taipei 101 Tower: field measurement and numerical analysis", *J. Struct. Eng.*, ASCE, **137**(1), 143-155.

Li, Z.N., Tang, J. and Li, Q.S. (2004), "Optimal sensor locations for structural vibration measurements", *Appl. Acoust.*, **65**, 807-818.

Lourens, E., Reynders, E., De Roeck, G., Degrande, G. and Lombaert, G. (2012), "An augmented Kalman filter for force identification in structural dynamics", *Mech. Syst. Signal Pr.*, **27**, 446-460.

Ma, C.K., Chang, J.M. and Lin, D.C. (2003), "Input forces estimation of beam structures by an inverse method", *J. Sound Vib.*, **259**(2), 387-407.

Ma, C.K., Tuan, P.C., Lin, D.C. and Liu, C.S. (1998), "A study of an inverse method for the estimation of impulsive loads", *Int. J. Syst. Sci.*, **29**(6), 663-672.

Mao, Y.M., Guo, X.L. and Zhao, Y. (2010), "A state space force identification method based on Markov parameters precise computation and regularization technique", *J. Sound Vib.*, **329**, 3008-3019.

Naets, F., Cuadrado, J. and Desmet, W. (2015), "Stable force identification in structural dynamics using Kalman filtering and dummy-measurements", *Mech. Syst. Signal Pr.*, **50-51**, 235-248.

Niu, Y., Fritzen, C.P., Jung, H. and Buethe, I. (2015), "Online simultaneous reconstruction of wind Load and structural responses-theory and application to canton tower", *Comput.Aid. Civil Infrastr. Eng.*, **30**, 666-681.

Nordström, L.J.L. (2006), "A dynamic programming algorithm for input estimation on linear time-variant systems", *Comput. Meth. Appl. Mech. Eng.*, **195**(44-47), 6407-6427.

Sanchez, J. and Benaroya, H. (2014), "Review of force reconstruction techniques" *J. Sound Vib.*, **33**, 2999-3018.

Simon, D. (2006), *Optimal State Estimation: Kalman, H Infinity, and Nonlinear Approaches*, John Wiley & Sons, New Jersey, USA.

Stevens, K.K. (1987), "Force identification problems (an overview)", *Proceedings of the SEM Conference on Experimental Mechanics*, Houston, TX, June.

Zhi, L. H., Li, Q.S., Wu, J.R. and Li, Z.N. (2011), "Field monitoring of wind effects on a super-tall building during typhoons", *Wind Struct.*, **14**(3), 1-31.

Zhi, L.H., Chen, B. and Fang, M.X. (2015), "Wind load estimation of super-tall buildings based on response data", *Struct. Eng. Mech.*, **56**(4), 625-648.

Zhi, L.H., Li, Q.S. and Fang, M.X. (2016), "Identification of wind loads and estimation of structural responses of super-tall buildings by an inverse method", *Comput. Aid. Civil Infrastr. Eng.*, **31**(12), 966-982.

CC